Trending and pattern recognition using the sphere-hardening phenomenon of signal multidimensional projection

François Léonard and Michel Gauvin

Institut de recherche d'Hydro-Québec – IREQ
1800 boulevard Lionel-Boulet, Varennes, QC, Canada J3X 1S1
{leonard.francois, gauvin.michel}@ireq.ca

Abstract

In trending and pattern recognition, the signal comprises a series of samples having a characteristic sequence, the so-called signature, repeatable from one measurement to another. Most of the non-repeatable part of the measurement comes from the measured intrinsic random contribution of the physical phenomenon, ambient noise, measurement system noise, and the temporal evolution of the physical phenomenon between two measurements. Projection of the signal of N-samples in a multidimensional space $\mathbf{R}^N$ for several measurements (Fig. 1) shows a distribution close to a hypersphere of radius r, where r corresponds to the measurement standard deviation. The estimated signature $\mathbf{S}_i$ is located at the center of the hypersphere. The measurements are grouped close to the hypersphere shell and the corresponding standard deviation around the radius r defines the "thickness" of the hypersphere shell also called the "hardness" of the hypersphere. Known as the "sphere hardening phenomenon", the hardness-to-radius ratio decreases with the increasing number N of dimensions. The measurement probability density appears as a function of the distance between the measurement and the hypersphere surface, with this distance related to the hardness. In the case of a large number of dimensions, the measurement distance to the hypersphere shell probability density function converges to a Laplace-Gauss model, thanks to the central limit theorem, and yields an analytical statistical formulation for the measurement likelihood. In contrast to some state-of-the-art monitoring algorithms, the proposed method gradually increases the sensitivity with the new measurements. The occurrence probability of a "false positive" (false alarm) appears constant from start-up through the steady state: the false-alarm rate at start-up is similar to that occurring in the steady state.

This paper explains the method, presents the mathematical developments and gives a sample application for monitoring substation equipment. In this application, the signal corresponds to the temporal envelope of the vibroacoustic operating noise. Data collected over a period of more than three years demonstrates the sensitivity and robustness of the method.

1   Background

For three decades, measuring systems and mass memory have increased according to Moore's Law, doubling in power every 18 months. However, the tools at our disposal for dealing with this information have not followed apace. Monitoring equipment is one of the applications that would benefit from this growth. In this area, the ideal solution for an average user is seen as a "black box with a red light" which tells him when his equipment has a behavior change. Equipped with a self-learning ability, this tool requires no configuration effort from the user [1-4]. At the opposite end of the spectrum, the "knowledge box with a red light" calls for the participation of experts for the tool set-up and the process modeling approach has some drawback [5,6]: the set-up is time-consuming and shortcoming in modeling implies diagnostic error; many processes are too complex for modeling.

The other issues are the "false positive" diagnostics or "false alarms" that undermine the credibility of a surveillance system. If the alarm levels are adjusted to avoid false alarms, the system loses its sensitivity and it is easy to miss a fault. Several methods have been put forward to solve this problem but some have been patented and are therefore not accessible without commercial agreement [2,3,7].

For a public utility like Hydro-Québec, the economic value of an accurate monitoring method is in the range of $100M/year. For example, a specialized monitoring service provider typically proposes a monitoring solution at a cost of $1000/year/channel. A hydroturbine has about 100 channels whereas a high-voltage (HV) substation (transformer and circuit-breaker monitoring) has several hundred channels. Since the Québec utility has 344 hydroturbines and 516 substations, the investment in R&D to find an alternative solution is justified.

We have developed a novel monitoring method using the "sphere-hardening phenomenon" well known in communication theory [8]. This method operates at the maximum likelihood. We will present the results collected from vibroacoustic measurements on equipment in an HV power substation. The impact of the method appears wider than the application domain of equipment monitoring. In fact, the method can be inserted in some existing solutions in mathematical statistics and operational research.

2 Signal characteristics and mathematical contexts

The method is applicable to signals comprising a series of samples having a characteristic sequence or signature repeatable from one measurement to another. Most of the non-repeatable part of the measurement comes from the random contribution of the phenomenon, ambient noise, measurement system noise and temporal evolution of the phenomenon between two measurements. The method enables variations of the measurements to be detected and quantified with respect to a signature, variations of a signature with respect to an initial signature, and a matching likelihood of a signature or a measurement with a specific signature pattern.

A measurement may be a time series, an envelope, an order power spectrum [9], a scalogram, a spectrogram, a 2D image, etc. In the context of the results presented below, the signal is the vibroacoustic envelope of a commutation occurring in an HV power switching device. Figure 1 illustrates 200 cumulated measurements by a time concatenation of successive histograms each corresponding to a time sample. The vibroacoustic signature appears constant for a small set of successive commutations, a given load and a given temperature. The evolution of a signature can be idle to progressive with the wear over numerous operations or sudden when a defect occurs.

In the proposed method, the measurement is projected in a multidimensional space $\mathbf{R}^N$. Many measurement projections are distributed within the shell of a hypersphere centered on the signature coordinates (Fig. 1). A measurement noise corresponds to a vector starting from the signature coordinates and pointing to the measurement coordinates. The average noise is the radius of the hypersphere. The method considers the total noise dispersion (i.e. the hypersphere radius) in $\mathbf{R}^N$ instead of a sample-to-sample local noise dispersion. The hypersphere shell has a thickness, also called hardness. The measurement population, the measurement dispersion and the number N of dimensions fix a standard deviation of the signature and the hypersphere thickness. The signature and hypersphere shell thickness values are estimated by the method and used to scale up the deviation amplitude between the measurements. In the case of a large number of dimensions, a measurement distance with respect to the hypersphere shell probability density function converges to a Laplace-Gauss modeling and yields an analytical statistical formulation for a measurement likelihood.
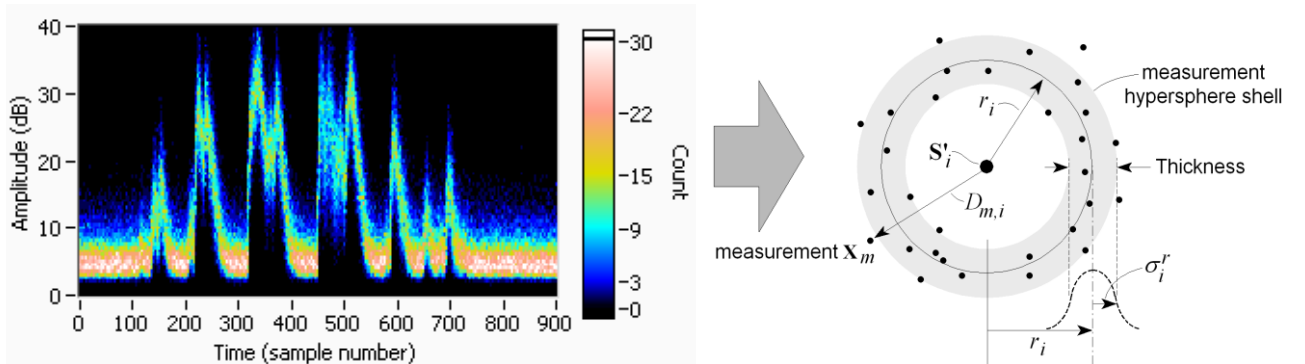
Figure 1: Time sample histograms from 200 vibroacoustic measurements (left) and artistic illustration of the hypersphere (right) of the measurements projected in a space $\mathbf{R}^N$. The hypersphere is centred on the estimated signature s corresponding to the measurement average.

The proposed method has its origin in the communication theory where a set of received symbols corresponds to a set of packed but not overlapped hyperspheres in a space $\mathbf{R}^N$. The communication channel capacity appears to be a function of the hypersphere packing density. This geometric visual representation facilitates the understanding of the noise contribution on the hypersphere radius, on the packing density and on the final channel capacity. Instead of many symbols, the proposed method considers mainly one symbol, the so-called "signature", and its corresponding hypersphere statistics. However, for diagnostic purposes, many signatures can be processed in a pattern recognition survey. The communication theory and proposed

method share the same idea: the likelihood of a measurement is estimated from its distance to the hypersphere shell scaled to the shell thickness. In the proposed method, if the monitored equipment has a new behavior, then the statistical likelihood of measurements of the new behavior exhibits a drop when compared to the signature estimated from measurements cumulated before the behavior change.

3   Mathematical formulations of the proposed method

For a signature S_i, assuming a repetitive pattern signature $S_{i,n}$ over different noise realizations where "n" is a subscript corresponding typically to time, frequency, wavelet scale or component order, let us consider an N- samples measurement (Fig. 1)

$$X_{mn} = S_{i,n} + n_{mn} , \ n \in [1, N] \tag{1}$$

where n_{mn} is the additive noise and m a subscript of the measurement realizations. Assuming a centered noise and many measurements of a same $S_{i,n}$ pattern, an $\mathbf{R}^N$ projection of the measurements exhibits a cluster centered on a point of $\mathbf{R}^N$ corresponding to the "i" signature estimate

$$\mathbf{S}_i^{'} = \left\{ S_{i,1}^{'}, S_{i,2}^{'}, ..., S_{i,N}^{'} \right\} \tag{2}$$

where the measurements

$$\mathbf{X}_m = \left\{ X_{m,1}, X_{m,2}, ..., X_{m,N} \right\} \tag{3}$$

are distributed close to a hypersphere shell (Fig. 1, right). Among different averaging options, a signature S_i may be estimated from a set of M measurements using a uniform average

$$\mathbf{S}_i \cong \mathbf{S}_i^{'} = \frac{1}{M} \sum_{m=1}^{M} \mathbf{X}_m . \tag{4}$$

This signature estimation is the first part of the four parts of "$\mathbf{R}^N$ signature statistics". In some trending applications, an updated estimated signature and other estimations are generated by a moving average process. A uniform average is presented here to keep the mathematical expressions short.

For example, for a Euclidian metric with uniform averaging, the measurement used to estimate the signature distance (Fig. 1, right -2)

$$D_{m,i} = \left| \mathbf{X}_m - \mathbf{S}_i^{'} \right| = \sqrt{\sum_{n=1}^{N} \left(X_{m,n} - S_{i,n}^{'} \right)^2} \tag{5}$$

has an expected mean for a set of M measurements. This set exhibits a cluster centered on the estimated signature $\mathbf{S}_i^{'}$, not on the real signature $\mathbf{S}_i$. The estimated signature appears in eq. 5 for two reasons. First, the real signature is unknown and, second, an internal error of the signature estimation must not appear at this step. Using eq. 5, an expected mean distance

$$r_i = \frac{1}{M} \sum_{m=1}^{M} D_{m,i} = \frac{1}{M} \sum_{m=1}^{M} \sqrt{\sum_{n=1}^{N} \left(X_{m,n} - S_{i,n}^{'} \right)^2} \ \text{ for } \mathbf{X}_m \in \text{cluster "}i\text{"}, \tag{6a}$$

or (on average less accurate)

$$r_i = \sqrt{\frac{1}{M} \sum_{m=1}^{M} D_{m,i}^2} = \sqrt{\frac{1}{M} \sum_{m=1}^{M} \sum_{n=1}^{N} \left(X_{m,n} - S_{i,n}^{'} \right)^2} \ \text{ for } \mathbf{X}_m \in \text{cluster "}i\text{"}, \tag{6b}$$

appears close to the noise vector length expectation $\sqrt{N \mathrm{E}\left(n_{mn}^2 \right)}$ where $\mathrm{E}(\ )$ is the expectation function. This estimation (r_i) will be referred to as the hypersphere radius. The double of the expected measurement standard deviation relative to hypersphere shell calculated with

$$\sigma_i^r = \sqrt{\frac{1}{M} \sum_{m=1}^{M} \left(r_i - \sqrt{\sum_{n=1}^{N} \left(X_{m,n} - S_{i,n} \right)^2} \right)^2} \tag{7a}$$

from measurements or estimated with

$$\sigma_i^r = r_i \cdot \sqrt{\frac{1}{2N}} \ \text{ (Gaussian white noise assumption)} \tag{7b}$$

from the estimated radius length will be referred to as the thickness (as shown in Fig. 1, right). In the case of Gaussian white noise, the estimated dispersion given with eq. 7b is less than that calculated with eq. 7a. The accuracy of the standard deviation of the measurement increases with the number M of measurements made.

For a small value of M, the estimation error on the standard deviation, i.e. the dispersion of the measurement dispersion

$$\left(\sigma_i''\right)^2 = \frac{\sigma_i'^2}{M-1} \quad \text{or} \quad \sigma_i'^r = r_i \cdot \sqrt{\frac{1}{2N \cdot (M-1)}} \quad \text{(Gaussian white noise assumption)} \tag{8}$$

should be also taken into account.

Figure 2: Illustration of the measurement $\mathbf{X}_m$, the estimated signature $\mathbf{S}_i'$ and their respective distance $D_{m,i}$ with measurement dispersions and *HRD* amplitude.
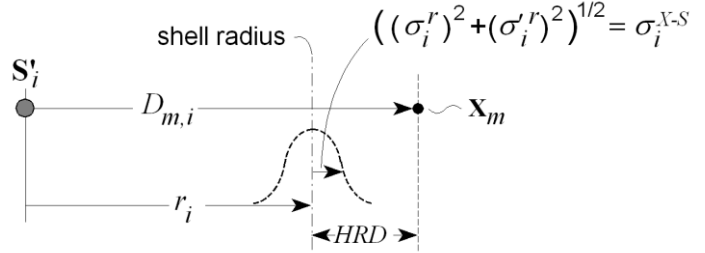
Referring back to Fig. 2, the measurement hypersphere radius r_i and shell thickness $2 \cdot \sigma_i^r$ are illustrated in $\mathbf{R}^N$. The "$\mathbf{R}^N$ measurement statistics" include the hypersphere radius r_i, the measurement standard deviation σ_i^r and the dispersion of the measurement dispersion $\sigma_i'^r$ (as shown in Fig. 2).

The measurement hypersphere shell thickness is a function of the metric (e.g. Euclidian), the measurement signal-to-noise ratio (SNR) and the number of time samples N. The ratio of the shell thickness over the hypersphere radius tends to 0 when $N \rightarrow \infty$. As mentioned, this phenomenon is called sphere hardening. Calculated using numerous noise samples, the expected distance $|\mathbf{X}_m - \mathbf{S}_i|$ appears constant and corresponds to the measurement hypersphere radius.

The estimated measurement hypersphere radius r_i is computed from a finite set on M measurement realizations. The estimated signature $\mathbf{S}_i'$ corresponds to the $\mathbf{R}^N$ coordinates that minimize the radius length (the estimated hypersphere radius being an underestimation of the real radius length). A fourth part of the "$\mathbf{R}^N$ measurement statistics" is formed from an estimated radius bias error

$$\varepsilon_i^s = r_i \cdot \sqrt{\frac{1}{M(M-1)}} \quad , \text{M} > 1, \tag{9}$$

that corresponds to an additional radius length observed for a measurement that is not included in the computed estimated signature: $\{\mathbf{X}_m : m \notin \{1, M\}\}$. This radius length bias is attributed to the average signature displacement when a new measurement is added to its estimation.

Referring to Fig. 2, in a preferred trending analysis, a last measurement is compared with a signature moving average and the latter, in turn, is compared with a reference signature established at the start of the monitoring. For the first comparison, when a measurement is near the hypersphere shell, the statistical deviation is governed by a ratio of a measurement-to-hypersphere shell distance over a measurement standard deviation, as expressed in eq. 7. Moreover, a dispersion of the measurement dispersion is taken into account. Figure 2 illustrates the different contributions involved in a deviation probability estimation. The distance difference $D_{m,i} - r_i$ when $\{\mathbf{X}_m : m \in \{1, M\}\}$ or $D_{m,i} - \left(r_i + \varepsilon_i^s\right)$ when $\{\mathbf{X}_m : m \notin \{1, M\}\}$ is related to the total dispersion of the measurement

$$\left(\sigma_i^{X-S}\right)^2 = \left(\sigma_i^r\right)^2 + \left(\sigma_i''\right)^2 \tag{10}$$

in order to obtain the probability density

$$\Omega\left(\mathbf{X}_m, \mathbf{S}_i\right) = \frac{e^{-\left(D_{m,i} - r_i - \varepsilon_i^s\right)^2 \Big/ 2\left(\sigma_i^{X-S}\right)^2}}{\sigma_i^{X-S} \sqrt{2\pi}} \tag{11}$$

for a large number N of dimensions, since for the contribution of numerous errors the hypersphere shell probability density function converges to a Laplace-Gauss modeling (central limit theorem [10]).

When the dispersion function is unknown or does not correspond to a possible analytical modeling, a histogram may be built using the collected measurements to estimate the probability density function

corresponding to the measurement population. A histogram interpolation may replace the modeling for further statistical formulations. Note that, for a large number of dimensions, the radius length distribution corresponds to the sum of numerous independent random variables; the central limit theorem states that the resulting distribution converges to a Laplace-Gauss distribution. With respect to the Laplace-Gauss modeling limitation, the hypersphere geometry shows a higher density of measurements on the inside of the shell than on the outside for a same distance to the shell (as shown in Fig. 1, right). The Laplace-Gauss approximation is good when the shell thickness (also seen in Fig. 1, right) is much smaller than the shell radius, corresponding to a large number N of dimensions. The modeling of Laplace-Gauss dispersion is valid for a large number of dimensions, facilitates implementation of the method and provides an analytical statistical predictability of the behavior (e.g., false-positive rate, probability of pattern matching).

In a warning system that monitors a drift magnitude exceeding k times (k>0), the standard deviation σ, knowing that

$$\text{erf}(z) = \frac{2}{\sqrt{\pi}} \int_0^z e^{-\xi^2} d\xi, \ \text{erf}\left(k/\sqrt{2}\right) = \frac{\sqrt{2}}{\sigma_n \sqrt{\pi}} \int_0^{k\sigma_n} e^{-x^2/2\sigma_n^2} dx \ \text{and}$$

$$\text{erfc}\left(k/\sqrt{2}\right) = 1 - \text{erf}\left(k/\sqrt{2}\right) \tag{12}$$

with the integration of probability density expressed in eq. 11, the probability of finding a measurement inside the shell exceeding the radius 202 of the cluster shell "i" by $k\sigma_i^{X-S}$ is

$$P(\mathbf{X}_m, \mathbf{S}_i)\big|_{(D_{m,i}-r_i)<k\sigma} = 0.5 + \int_0^{+k\sigma_i^{X-S}} \frac{e^{-x^2/2\left(\sigma_i^{X-S}\right)^2}}{\sigma_i^{X-S}\sqrt{2\pi}} \cdot dx = 0.5 + 0.5 \cdot \text{erf}\left(k/\sqrt{2}\right). \tag{13}$$

The probability of finding a measurement outside the shell $r_i + k\sigma_i^{X-S}$ is

$$P(\mathbf{X}_m, \mathbf{S}_i)\big|_{(D_{m,i}-r_i)>k\sigma} = 0.5 - 0.5 \cdot \text{erf}\left(k/\sqrt{2}\right). \tag{14}$$

The probability of finding a measurement inside the shell $r_i - k\sigma_i^{X-S}$ is

$$P(\mathbf{X}_m, \mathbf{S}_i)\big|_{(D_{m,i}-r_i)<-k\sigma} = 0.5 - 0.5 \cdot \text{erf}\left(k/\sqrt{2}\right). \tag{15}$$

The probability of finding a measurement inside and outside the shell boundaries $r_i \pm k\sigma_i^{X-S}$ is respectively

$$P(\mathbf{X}_m, \mathbf{S}_i)\big|_{|D_{m,i}-r_i|<k\sigma} = 1 - 2 \cdot \left(0.5 - 0.5 \cdot \text{erf}\left(k/\sqrt{2}\right)\right) = \text{erf}\left(k/\sqrt{2}\right) \ , \text{and} \tag{16a}$$

$$P(\mathbf{X}_m, \mathbf{S}_i)\big|_{|D_{m,i}-r_i|>k\sigma} = 2 \cdot \left(0.5 - 0.5 \cdot \text{erf}\left(k/\sqrt{2}\right)\right) = \text{erfc}\left(k/\sqrt{2}\right). \tag{16b}$$

A distance between a measurement and the S_i hypersphere shell is referred to herein as a hypersphere radius deviation (*HRD*) (Fig. 2) defined as

$$HRD_{m,i} = D_{m,i} - r_i \ \text{when} \ \{\mathbf{X}_m : m \in \{1, M\}\} \tag{17a}$$

and, when a measurement $\mathbf{X}_m$ does not contribute to the estimated signature,

$$HRD_{m,i} = D_{m,i} - \left(r_i + \varepsilon_i^s\right) \ \text{when} \ \{\mathbf{X}_m : m \notin \{1, M\}\} \tag{17b}$$

For example, in the case of a trending analysis, when the last measurement is compared with a signature average, an alarm may be set by fixing a k maximum value referred to as k_{max}. An alarm occurs when

$$k \geq k_{\max} \tag{18}$$

with

$$k^2 = \left(HRD_{m,i} \big/ \sigma_i^{X-S}\right)^2. \tag{19a}$$

or

$$k^2 = \frac{(D_{m,i}-r_i)^2}{\left(\sigma_i^{X-S}\right)^2} = \frac{(D_{m,i}-r_i)^2}{r_i^2 \cdot \left(\frac{1}{N} + \frac{1}{N \cdot (M-1)}\right)} = \left(\frac{D_{m,i}}{r_i} - 1\right)^2 \bigg/ \left(\frac{1}{N}\left(1 + \frac{1}{M-1}\right)\right), M>1 \tag{19b}$$

5

when rewritten in terms of measurement distance to estimated signature $D'_{m,i}$, average measurement distance r_i, a number M of measurements and a number N of dimensions. The false-alarm rate is defined by eq. 16b with $k = k_{max}$. The method thus uses the ratio expressed in eq. 19 with a single statistical parameter k_{max} to monitor the whole measurement pattern. At start-up, the small M value increases the dispersion (eqs. 8 and 9). An HRD value observed at start-up appears less significant than the same deviation observed after the collection of more measurements. From eq. 9b, $k=0$ when $M=1$: the zero-sensitivity reflects the unavailable statistic with only one measurement available. For a small number of measurements, the k value increases rapidly with the contribution of each new measurement. The $1+1/(M-1)$ factor in eq. 9b acts as a sensitivity reducer during start-up of the statistical estimation process. Since the sensitivity gradually increases with the new measurements, the occurrence probability of "false positive" (false alarm) appears constant from start-up through steady state.

When the combined deviation of a plurality of L measurements is considered from the signature i, the corresponding k value can be estimated from the average HRD value. Less accurate,

$$k^2 = \frac{1}{L} \sum_{l=1}^{L} \left(\frac{HRD_{l,i}}{\sigma_i^{X-S}} \right)^2 = \frac{1}{L} \sum_{l=1}^{L} k_l^2 \tag{20}$$

is another estimation expression for combining many measurements. The same expression can be used to combine a plurality of L measurement deviations from the same number of corresponding signatures projected in different $\mathbf{R}^N$ subspaces when

$$k_l = \frac{HRD_l,i}{\sigma_l^{X-S}} . \tag{21}$$

Note that in the latter case, since k is dimensionless, the engineering unit corresponding to the hypersphere subspace l can be fixed arbitrarily. For example, using eqs. 20 and 21, it is possible to mix the deviation of a vibration reading with the deviation observed on multiple temperature readings.

Figure 3: N-dimensional illustration of the trend of a signature captured at four different times.
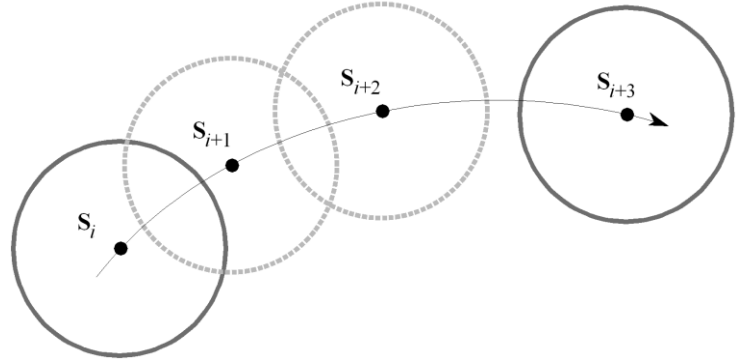
Figure 4: N-dimensional illustration of the trending of a signature captured at two different times where the measurement dispersion appears larger for the last signature $\mathbf{S}_{i+1}$.
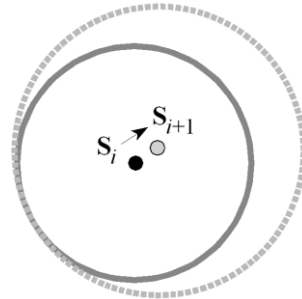
Referring to Fig. 3, a trend in a signature may be considered as successive signatures starting from an initial signature. Different possibilities exist for the evolution step between two successive signatures. A first possibility is easier to detect and corresponds to the case of (Si,Si$_{+2}$), (Si,Si$_{+3}$) and (Si$_{+1}$,Si$_{+3}$) comparisons. The comparisons (Si,Si$_{+1}$) and (Si$_{+1}$,Si$_{+2}$) are more difficult since two hyperspheres are overlapping; some measurements may be shared by both clusters. The problem is a signature-to-signature discrimination and distance estimation. Figure 4 shows the worst case where the signature step is less than the noise radius and

where the noise fluctuation is also in the same amplitude range as the step. In the case illustrated, the measurement dispersion appears larger for the last signature S_{i+1}. These illustrations may also be applied for pattern recognition where a running signature is compared to a signature extracted from a database. It will be seen that the $\mathbf{R}^N$ representation of the signal allows discrimination of two signatures even if the signature hyperspheres overlap.

Referring to Fig. 5, the coordinates of the estimated signature $\mathbf{S}_i'$ in $\mathbf{R}^N$ appear to be a function of the available corresponding measurements (as shown in Fig. 1, right). Different measurement sets yield different estimated signature coordinates. There exists an estimation bias $E\left|\mathbf{S}_i - \mathbf{S}_i'\right|$ as well as an expectation for the bias dispersion. As illustrated on the left, two signature estimations $\mathbf{S}_i'$ and $\mathbf{S}_j'$ are located on their respective signature hyperspheres, both centered on their common denoised signature $\mathbf{S}$. As second part of the "$\mathbf{R}^N$ signature statistics", the estimated signature $\mathbf{S}_i'$ hypersphere radius

$$r_i^s = \sqrt{\frac{1}{M} \cdot \frac{1}{M} \sum_{m=1}^{M} \sum_{n=1}^{N} \left(X_{m,n} - S_{i,n}'\right)^2} = \sqrt{\frac{1}{M} \cdot r_i^2} = r_i \cdot \sqrt{\frac{1}{M}} \tag{22}$$

decreases when the number of measurements increases. As a third part of the "$\mathbf{R}^N$ signature statistics", the signature dispersion (as shown in Fig. 7)

$$\sigma_i^s = r_i \cdot \sqrt{\frac{1}{2N(M-1)}} \quad , M>1 \tag{23}$$

decreases when the number of dimensions increases. The estimated radius bias error ε_i^s (as shown in Fig. 7) given by eq. 9 is a fourth part of the "$\mathbf{R}^N$ signature statistics" and corresponds to an internal error of the signature estimation location in $\mathbf{R}^N$.

Figure 5: Schematic diagram illustrating hyperspheres of two signatures related to a same denoised signature and a hypersphere corresponding to signature subtraction.
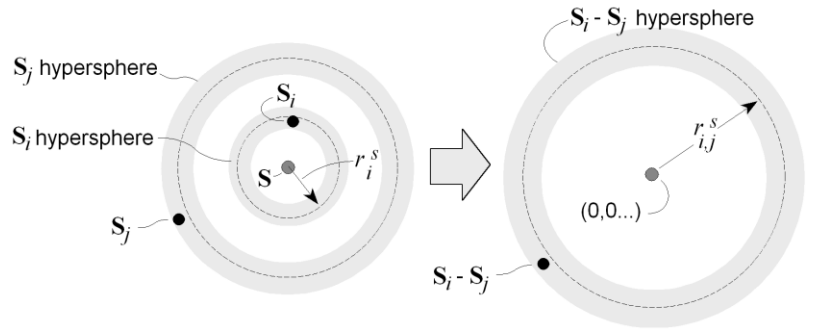
Note that σ_i^s has the same mathematical expression as the "dispersion of the measurement dispersion" $\sigma_i^r{}'$ (eq. 8). In some special cases, these two estimations do not correspond to the same dispersion phenomenon: For example, considering a merging of two signatures estimated with different noise amplitudes, the dispersion σ_i^s decreases when $\sigma_i^r{}'$ may increase with the merging.

The distance between two hyperspheres can be illustrated as one hypersphere centered on a zero-origin coordinate (Fig. 5, right). The hypersphere radius length of the signature distance

$$r_{i,j}^s = \sqrt{\left(r_i^s\right)^2 + \left(r_j^s\right)^2} \tag{24a}$$

is the quadratic sum of the respective hypersphere radius lengths. Including the internal error in the radius length, the signature distance hypersphere radius length 214 can be rewritten

$$r_{i,j}^{s\varepsilon} = \sqrt{\left(r_{i,j}^s\right)^2 + \left(\varepsilon_i^s\right)^2 + \left(\varepsilon_j^s\right)^2} \ . \tag{24b}$$

A distance between two signatures is referred to herein as a hypersphere signature deviation (*HSD*) defined as

$$HSD_{i,j} = D_{i,j} - \sqrt{\left(r_{i,j}^s\right)^2 + \left(\varepsilon_i^s\right)^2 + \left(\varepsilon_j^s\right)^2} = D_{i,j} - r_{i,j}^{s\varepsilon} \quad . \tag{25}$$

Figure 6 illustrates a signature-to-signature comparison. The estimated signature $\mathbf{S}_i'$ hypersphere radius given in eq. 22 is used in the case of a uniform average. For a moving average signature with non-uniform weighting, the radius has a different mathematical expression. Whatever the mathematical expression of averaging and the corresponding dispersion, the total dispersion between signatures

$$\left(\sigma_{i,j}^{S-S}\right)^2 = \left(\sigma_i^s\right)^2 + \left(\sigma_j^s\right)^2 \tag{26}$$

is related to *HSD* in order to obtain the probability density

$$\Omega\left(\mathbf{S}_i, \mathbf{S}_j\right) = \frac{e^{-HSD_{i,j}^2 / 2\left(\sigma_{i,j}^{S-S}\right)^2}}{\sigma_{i,j}^{S-S}\sqrt{2\pi}} \tag{27}$$

in the case of a Laplace-Gauss dispersion modeling. Note that, when $\sigma_{i,j}^{S-S} << r_{i,j}^s$, the $\mathbf{R}^N$ representation of the signal may allow discrimination of two signatures even if the signature hyperspheres overlap. From eq. 12 and integrating the probability density expressed in eq. 27, the probability of finding the moving-average signature inside the $k \cdot \sigma_{i,j}^{S-S}$ limit is

$$P\left(\mathbf{S}_i, \mathbf{S}_j\right)\Big|_{D_{i,j} < k\sigma} = \int_0^{+k\sigma_{i,j}^{S-S}} \frac{e^{-HSD_{i,j}^2 / 2\left(\sigma_{i,j}^{S-S}\right)^2}}{\sigma_{i,j}^{S-S}\sqrt{2\pi}} \cdot dx = \mathrm{erf}\left(k/\sqrt{2}\right) \quad . \tag{28}$$

For example, in a signature-to-signature comparison, an alarm may be set by fixing a k maximum value k_{max}. An alarm occurs when $k \geq k_{\max}$ with

$$k = HSD_{i,j} \Big/ \sigma_{i,j}^{S-S} \quad . \tag{29}$$

The false alarm rate is defined by eq. 16b with $k = k_{max}$. The method thus uses the ratio expressed in eq. 29 with a single statistic parameter k_{max} to monitor the whole signature pattern matching.

Figure 6: Illustration of the estimated signature $\mathbf{S}_i'$ to estimated signature $\mathbf{S}_j'$ distance $D_{i,j}$ with the total signature dispersion $\sigma_{i,j}^{S-S}$ and the hypersphere-to-signature distance (*HSD*).
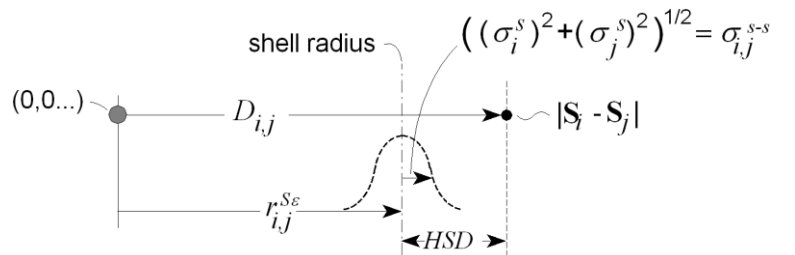
Figure 7 illustrates a simulated example of the sphere-hardening phenomena occurring with the increased dimensionality. Four different noise sources (Gaussian, linear, quadratic and cubic) are selected randomly for the N dimensions with different amplitudes in the same range. For a few dimensions, the *HRD* shows a probability density function which does not match the Laplace-Gauss distribution well. For dimensions having different noises in the same dispersion amplitude range, a Gaussian match is observed for as low as 10 dimensions. The simulation case of $N= 900$ (Fig. 8, bottom) corresponds to the 900 time samples vibroacoustic measurement illustrated in Fig 1.
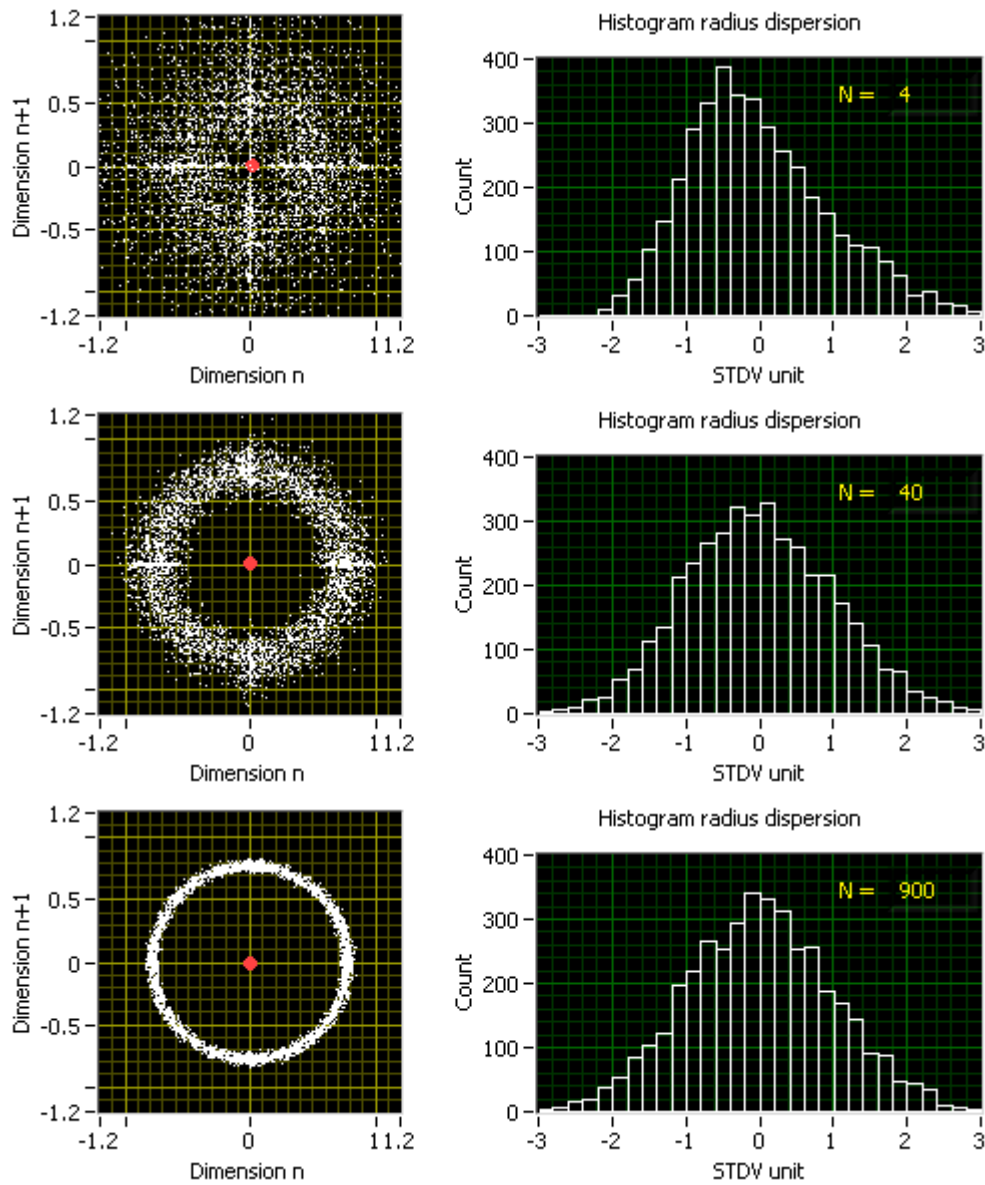
Figure 7: Illustration of the projection in 2D of 4000 noise measurements for *N*= 4, 40 and 900 dimensions. Radius length dispersion histograms are presented in standard deviation (STDV) bin units.

4   Trending of vibroacoustic commutation envelope signal

This section compares the application of the novel method against the classic N σ threshold (normal law) alarm limit method by using a subset of a field experience measurements. For the last three years, a vibroacoustic data acquisition system has been acquiring vibroacoustic commutation signals from power transformer equipment in an electrical substation. Signal processing is applied to the vibroacoustic waveform to extract its envelope and the envelope is then processed by the two methods.

The case we present is a comparison of the two methods applied to the trending of vibroacoustic measurements. First we compute the results of both methods without any alteration of the measurements. We then compute the results of the two methods inserting a state change that occurs linearly with time on the real measurements. In this comparison we use 328 measurements of a specific movement of power transformer equipment. Figure 8 shows the 328 overlapping vibroacoustic envelope measurements.

9
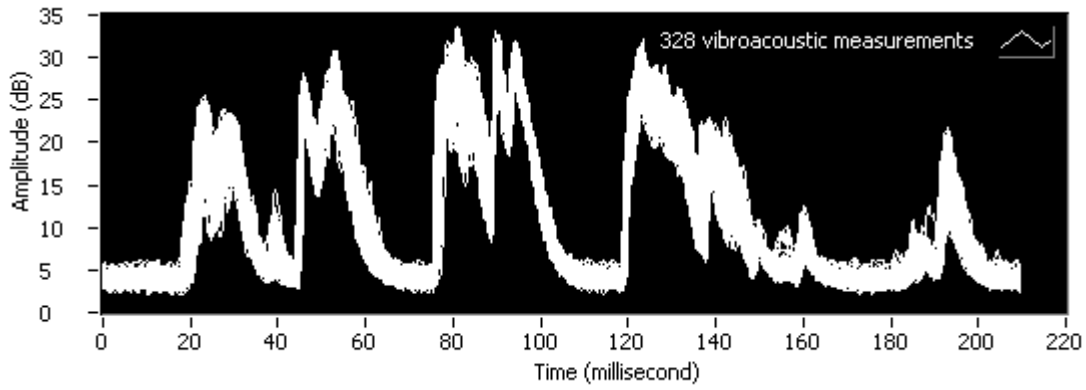
Figure 8: Overlapping vibroacoustic measurements from field experience.

Figure 9 shows the results of the two methods without any alteration to the measurements. At first sight it may be observed that the *HSD* (eq. 25) results look smoother than the traditional method. The reason for this is that the *HSD* makes an overall assessment of the comparison between the reference signature and the moving-average signature as opposed to the traditional method which makes a local assessment of the comparison by taking the worse sample deviation. It may be observed that there is no over-limit when using either method. The normal wear from the last three years' operation of a piece of equipment awaiting a major overhaul explains the trend observed in both graphs in Fig. 9.
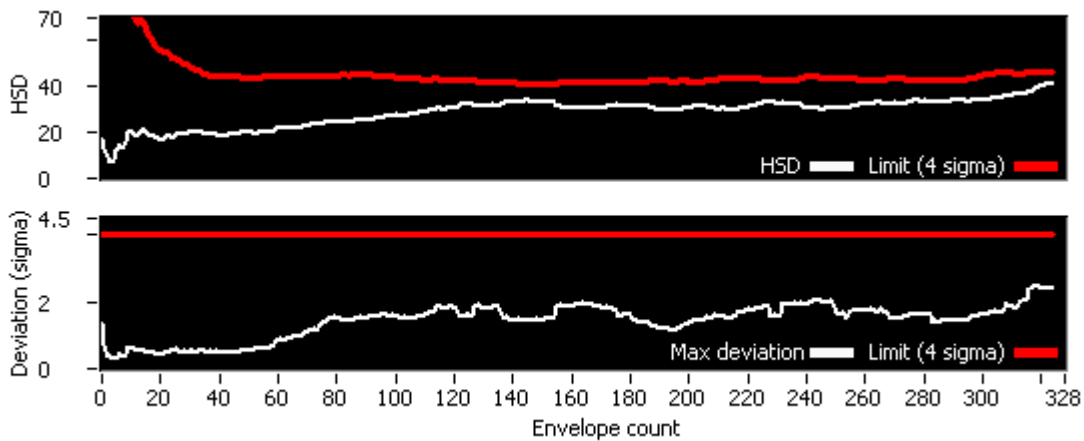
Figure 9: Results of the two methods without any alteration to the measurements.

Figure 10 shows the state change introduced in the measurements in order to simulate a trending towards an imminent failure in the equipment mechanism. The simulation of the state change works as follows: whenever a new measurement comes in, it is modified with the amplitude weights and timing weights (see Fig. 10), which are computed linearly based on the number of measurements that the state change takes to develop. In this simulation the state change starts at measurement #40 and develops over 288 measurements. Figure 11 shows the results of the simulation. With the use of the novel method presented here, the trend is easily observed as exceeding the limit. Furthermore, the limit is created dynamically and stabilizes as the number of measurements increases. With the traditional method, one can see a semblance of a trend but not as pronounced with the new method. Finally, the traditional method never exceeds the alarm threshold.
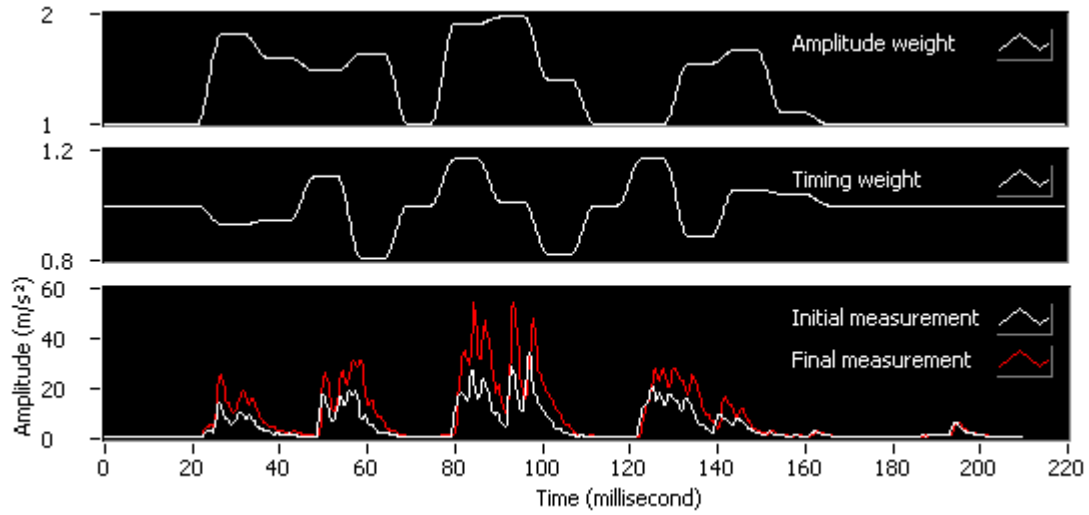
Figure 10: Simulation of a state change in the monitored equipment.
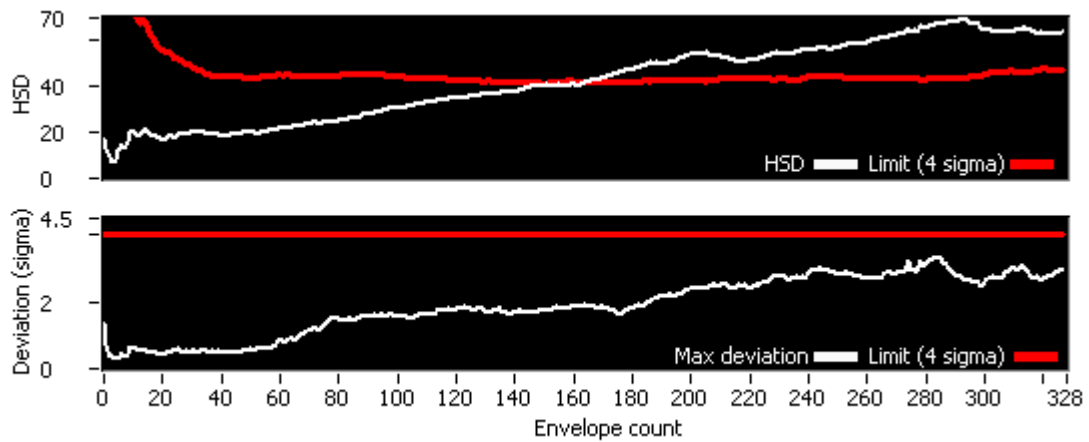
Figure 11: Results of the two methods with a linear state change on the measurements.

5 Conclusion

The $\mathbf{R}^N$ signal projection allows the sphere-hardening phenomenon to be used in pattern matching and pattern pursuit of a characteristic sequence repeatable from one measurement to another. This signal sequence can originate from a temporal sequence, e.g., an order power spectrum, a scalogram or a concatenation of measurement channels. This paper has given the sets of equations for matching, i.e. signature-to-signature comparison, and for pursuit, i.e. signature trending considering a new measurement. This method is recommended in the context of many dimensions (>4) and many measurements (>30). For a set of N non-cross-correlated signal dimensions, the accuracy increases by a factor of $\sqrt{N}$. For a large number of dimensions (>30), the probability density function of the measurements contained in the hypersphere shell converges to a Laplace-Gauss model: the matching and pursuit likelihood is described by the well-known Laplace-Gauss formulation facilitating the implementation and understanding of the alarm algorithm. In our context, namely the trending of a vibroacoustic time signal signature (900 samples), the method yields a significant increase in the ratio of sensitivity over a false-alarm rate compared to the classic standard deviation method for simulated defects on real measurements. Moreover, the sensitivity of the method is self-learning: the sensitivity gradually increases with the new measurements and the occurrence probability of "false positives" (false alarms) appears constant from start-up through the steady state. For the monitoring system implemented, this method seems to be the only acceptable solution.

References

[1] W.R.A. Ibrahim, M.M. Morcos, *An adaptive fuzzy self-learning technique for prediction of abnormal operation of electrical systems*, IEEE Transactions on Power Delivery (2006), Vol. 21 , No. 4, pp. 1770–1777.

[2] Stephan W. Wegerich, David R. Bell, Xiao Xu, *Global state change indicator for empirical modeling in condition based monitoring*, Patent US 6,859,739 B2, 2005.

[3] Stephan W. Wegerich, *Complex signal decomposition and modeling*, Patent US 8,239,170 B2, 2012.

[4] Jingjing Liu; Shouqi Yuan ; Congli Mei ; Yue Tang ; Jianping Yuan, *Detecting abrupt changes based on dynamic analysis of similarity for rotating machinery fault prognosis*, IEEE Control and Decision Conference (CCDC)(2010), pp. 3924 – 3927.

[5] Fu Yang; Zhang Liang, *Comprehensive method detecting the status of the transformer based on the artificial intelligence*, International Conference on Power System Technology (2004), Vol. 2, pp. 1638 - 1643

[6] M. Ahfaz Khan; A.K. Sharma, R. Saxena, *Expert System for Power Transformer Condition Monitoring and Diagnosis*, International Conference on Power Electronics, Drives and Energy Systems (2006). PEDES '06.

[7] Stephan W. Wegerich, Andre Wolosewicz, Xiao Xu, James P. Herzog, Robert Matthew Pipke, *Automated model configuration and deployment system for equipment health monitoring*, patent US 7640145 B2, 2009.

[8] C. Shannon, *Communication in the Presence of Noise*, Proceeding of the IRE (1949), Vol. 37, No.1, pp. 10–21.

[9] K. R. Fyfe and E. D. S Munck, *Analysis of computed order tracking*, Mechanical Systems and Signal Processing (1997), Volume 11, No. 2, pp. 187–205.

[10] Pierre-Simon Laplace, *Mémoire sur les approximations des formules qui sont fonctions de très-grands nombres, et sur leur application aux probabilités*, Mémoires de la Classe des sciences mathématiques et physiques de l'Institut de France, 1809, pp. 353-415, 559-565.